Green synthesis of TiO_2 NPs from Moringa Oleifera leaf extract for Removal of Dye and Drug from an Aqueous Solutions

Meera R. Popaliya [1], Arvnabh Mishra [2], Keval R. Rana [3], Kinnari Bhatt *

(ORCID Id: 0000-0002-0050-5493)

*[1, *] Department of Organic Chemistry, Institute of Science & Technology for Advanced Studies & Research (ISTAR), The Charutar Vidya Mandal (CVM) University, Vallabh Vidyanagar - 388120, Gujarat, India*

[2] Department of Chemistry, Shri Govind Guru University, Vinzol-388713, Gujarat, India

[3] Hindusthan Speciality Chemicals Limited, Bharuch – 393110, Gujarat, India

(Corresponding Author: Dr. Kinnari Bhatt)

Abstract

Presently, scholars are highly interested in the environmentally sustainable synthesis of nanomaterials due to their cost-effectiveness, low energy consumption, reproducibility, and absence of contamination. Titanium dioxide nanoparticles (TiO_2 NPs) were synthesized in an environmentally friendly manner using leaf extract. The TiO_2 NPs were subsequently analyzed using FTIR, EDX, XRD, TEM, BET and FESEM. The generation, size, and shape of the TiO_2 NPs were all confirmed using spectroscopic and microscopic methods. The photocatalytic efficacy of the produced TiO_2 NPs was investigated by decomposing Methylene blue dye (MBD) and Gatifloxacin (GTF). Additionally, this study investigates the effects of various adsorbent doses, pH, concentrations, stirring speed, temperatures, and adsorption times on the adsorption efficiency of TiO_2 NPs. The adsorption investigations indicate that the maximal adsorption capacity of MBD and GTF was 145.77 mg/g and 91.32 mg/g, respectively.

Keywords Adsorption, Gatifloxacin, Green approach, Methylene blue dye, TiO_2 NPs

Abbreviation

AOD Acridine orange dye

BET Brunauer-Emmett-Teller

BJH Barrett-Joyner-Halenda

CVD Crystal violet dye

EDX Energy dispersive X-ray spectroscopy

FESEM Field emission Scanning electron microscope

FTIR Fourier transform infrared spectroscopy

GTF Gatifloxacin

HCl Sodium chloride

HR-TEM High-Resolution Transmission Electron Microscope

MBD Methylene blue dye

MO Moringa oleifera

NaOH Sodium hydroxide

POPs Persistent organic pollutants

TiO_2 NPs Titanium dioxide nanoparticles

TTIP Titanium tetra iso-propoxide

XRD X-ray Diffraction

1. Introduction

Environmental safety is now a serious global issue. One of the most pressing challenges here is water pollution. Different discharges, such as heavy metals, dyes, drugs, and pesticides, reach various water bodies and contribute significantly to water pollution. Synthetic dyes and pigments cause contamination of water sources [1, 2]. Rapid industrialization and global modernity have led to the unregulated use and discharge of persistent organic pollutants (POPs) into the environment. The environment classifies POPs as persistent chemicals, and their potential for long-range transport, tendency to bioaccumulate in ecosystems, and impact on human health have raised significant concerns [3].

Many industries, including cosmetics, pharmaceuticals, leather, polymers, and textiles, use cationic dyes as colorants [4]. Waste generation and inappropriate disposal are among the risks associated with industrial activities. The textile industry accounts for 20% of total world pollution [5]. The unpredictable release of these dyes into the aquatic environment may affect marine ecosystems [6, 7]. Coloured effluent is a byproduct of the dye synthesis process, accounting for about 10–15% of the dye [8]. Cationic dyes with aromatic structures, such as MBD, CVD, and AOD, are important constituents in many industries, including wood, cotton, and silk dyeing, textiles, printing, pesticides, pulp and paper, cosmetic goods, food processing, and research facilities [9].

POPs, like antibiotics, have received a lot of attention since even modest amounts of antibiotics may have serious side effects. Antibiotics are widely used in various industries, including agriculture, cattle production, and healthcare [10, 11]. GTF is an antibiotic used to treat bacterial infections [12]. GTF is biochemically active, persistent, and accumulates quickly in the environment. Improper GTF disposal may pollute water bodies, leading to the growth of antibiotic-resistant bacteria and harming both human and aquatic life [13, 14]. Fig. 1 illustrates the various risks associated with industrial effluent. Therefore, we must treat industrial effluent to eliminate dyes and pharmaceuticals before dumping it into bodies of water.

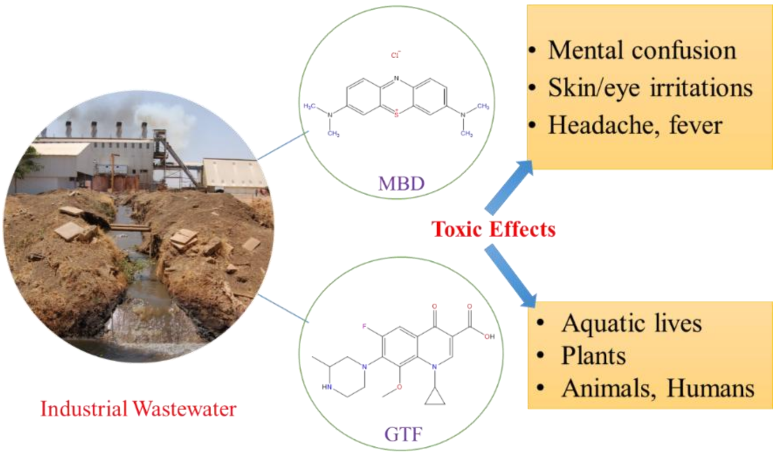

Fig.1 Harmful effects of dye & drug pollutants

There are two distinct methods for producing nanoparticles. They employ both top-down and bottom-up strategies. Top-down techniques investigate the process of converting bulk materials into nanoparticles, while bottom-up approaches focus on atoms combining to produce bulk nanoparticles [15]. TiO_2 nanoparticles were produced using a variety of chemical and physical processes, including sol-gel [16, 17], hydrothermal [18], microwave irradiation [19], ball milling [20], co-precipitation [21], and wet chemical procedures [22]. Physical methods used included arc discharge, electron beam lithography, ion implantation, inert gas condensation, mechanical grinding, milling, spray pyrolysis, and vapor phase synthesis. These approaches involve the use of very toxic chemicals, high temperatures, and stabilizing reagents that are harmful to the environment and humans. The most common materials utilized to create TiO_2 nanoparticles were titanium IV alkoxide, titanium butoxide, titanium tetra isopropoxide (TTIP), and titanium tetrachloride ($TiCl_4$). Titanium tetrachloride is the most toxic and caustic of the precursors, yet titanium (IV) alkoxide is costly and soluble in organic solvents [23].

Conversely, the green method is the most advantageous choice for nanoparticle synthesis because it is more ecologically friendly and sustainable because it doesn't need any hazardous chemicals, high temperatures, or sophisticated equipment (Fig. 2). People often use the green synthesis process to produce nanoparticles that contain proteins, sugars, phenolic acids, terpenoids, flavonoids, and polyphenols. The plant's peels [24], leaves [25], flowers, roots [26], stems, seeds, and fruits [27] were among the components used to extract the crude extract. These secondary metabolites act as reducing agents, transforming metal ions into nanoparticle-sized metal oxides. Nanoparticles made from green processes are also safe for the environment and work well to stop oxidative stress, genotoxicity, and changes related to apoptosis [28, 29]. Acorus calamus leaf [30], Terminalia Catappa - Carissa Carandas fruits [31], Nyctanthes arbor-tristis leaf [32], Solanum trilobatum [33], Annona squamosal [34], Catharanthus roseus leaf [35], Jatropha curcas [36], Eclipta prostrate plant extracts [37], and Calotropis gigantean flower extract [38] are just a few examples of the plant extracts used in the green synthesis of TiO_2 nanoparticles.

Fig.2 Benefits of green synthesis of NPs [39]

The present work focuses on the green synthesis technique for producing titanium dioxide (TiO_2) nanoparticles from Moringa oleifera leaf extracts. The following sections thoroughly explain the experimental method, characterizations, and obtained results. This is the first research that uses green-produced TiO_2 NPs as an adsorbent to remove MBD and GTF from an aqueous solution.

2. Experimental

2.1. Materials

Moringa Oleifera (Drumstick) leaves were obtained in the surrounding region (Vallabh Vidyanagar, Anand, Gujarat, India). Suvidhinath Laboratories (Sulab) in Vadodara, India, supplied titanium tetra isopropoxide (TTIP), sodium hydroxide (NaOH), sodium chloride (HCl), and methylene blue dye (MBD). The Department of Chemistry provided Gatifloxacin (GTF). We used the reagents without further purification.

2.2. Methods

2.2.1. Preparation of adsorbent

2.2.1.1 Synthesis of leaf extract

We washed the fresh leaves of Moringa oleifera (MO) plants with distilled water and dried them in the shade. We preserved the dried leaves in a sealed container to use later. 1 gm of leaves was put in a beaker with 100 ml of distilled water. The solution was heated on a burner at 70°C for 30 minutes. Later, we purified the fluid and used it in research.

2.2.1.2 Synthesis of TiO_2 NPs

We employed a magnetic stirrer to continuously stir a solution comprising 1 M TTIP and 50 ml of double-distilled water at room temperature for a duration of 30 minutes. Next, we applied 25 mL of leaf extract dropwise to the TTIP and double-distilled water solution. We completely mixed the solutions with a high-speed magnetic stirrer and maintained the temperature at 60 °C for 3 hrs (Fig. 3). The major method to produce TiO_2 particles is the hydrolysis of TTIP. Leaf extract can be used as a stabilizing or capping agent to stop TiO_2 particles from sticking together. This makes it easier to get the size and shape that is wanted. We then cooled the mixture to room temperature. We filtered out the orange residue using Whatman filter paper and then dried it in an oven. The residue was then put in a muffle furnace and calcined at 500°C for 1 hr. After calcination, we cooled the white TiO_2 particles and analyzed them.

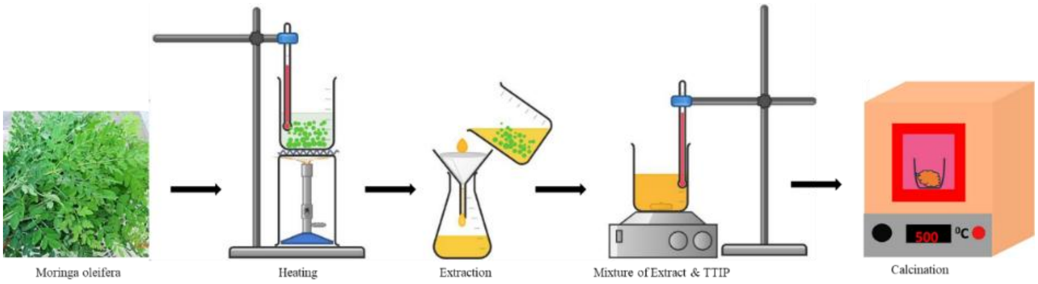

Fig 3 Flow diagram: Green synthesis of TiO_2 NPs

2.2.2 Preparation of adsorbates

This study used MBD and GTF as adsorbates, with maximum wavelengths of 665 and 285 nm, respectively. Table 1 displays the adsorbates' structures, chemical formulas, and IUPUC names. The molecular weights of the chemical compounds MBD (CI No. 52015) and GTF (CID 5359) are 319.85 and 375.4 g/mol, respectively. It has several applications in biology, chemistry, and medicine. To prepare a stock solution of the dye and drug, dissolve 0.1g of the substance in 1 L of distilled water. We evaluated the adsorbate concentration in the aqueous solution using UV spectrophotometry (UV-VIS SPECTROPHOTOMETER 1800). This investigation used only analytical-grade chemicals and distilled water.

Table 1 Basic information on adsorbates.

Adsorbates	**Structure**	**Chemical formula**	**IUPAC name**
MBD	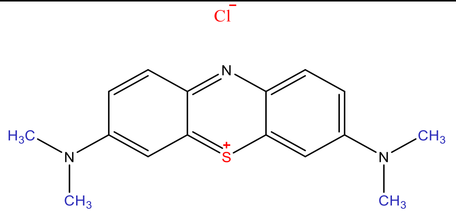	$C_{16}H_{18}ClN_3S$	[7-(dimethylamino) phenothiazin-3-ylidene]-dimethylazanium chloride
GTF	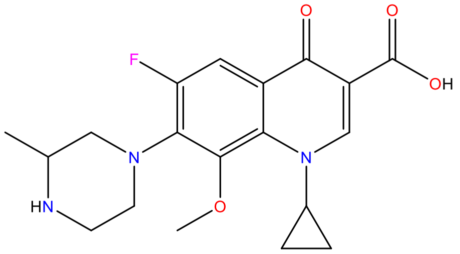	$C_{19}H_{22}FN_3O_4$	1-Cyclopropyl-6-fluoro-8-methoxy-7-(3-methylpiperazin-1-yl)-4-oxo-quinoline-3-carboxylic acid

2.2.3 Characterization

To analyze the infrared spectra of TiO_2 NPs, we used Fourier transform infrared spectroscopy (PerkinElmer, Spectrum two) for both the samples before and after adsorption. We analyzed the surface morphology of the TiO_2 NPs using a field emission scanning electron microscope (HITACHI, Japan, SU8010 Series), and analyzed the crystal structure utilizing a high-resolution transmission electron microscope (JEOL, JEM 2100 Plus). We analyzed the elements in TiO_2 NPs before and after adsorption using energy-dispersive X-ray spectroscopy. (Hitachi, Japan/ESEM EDAX XL 30). The X-ray diffractometer (Panalytical X-Pert Pro) offers valuable insights through its X-ray diffraction analysis capabilities. This technique allows for the identification and quantification of crystalline phases. We measured the surface area of TiO_2 NPs using Brunauer-Emmett-Teller analysis with Quantachrome equipment (Autosorb IQ, USA).

2.3 Equations

2.3.1 % Adsorption

Equations (1) and (2) allowed us to quantify the adsorbates' adsorption on the adsorbent in terms of the amount adsorbed (mg/g) and the percentage of dye and drug adsorption,

$q_e = (C_i - C_e) * {}^{v}/_{w}$ (1)

$\% Adsorption = {}^{(C_i - C_e)}/_{C_i} \times 100$ (2)

In this equation, qe represents the equilibrium adsorption capacity (mg/g), Ci represents the initial concentration of the adsorbate solution (mg/L), Ce represents the equilibrium concentration of the adsorbate, v represents the volume of the aqueous solution (ml), and w represents the mass of the adsorbent (gm).

2.3.2 Adsorption isotherm

The linear equations for isotherm data suggested by Langmuir, Freundlich, and Temkin models are represented by equations (3), (4), and (5), respectively.

$\frac{1}{q_e} = \frac{1}{K_L q_{max}} \frac{1}{C_e} + \frac{1}{q_{max}}$ (3)

$Log q_e = Log K_f + \frac{1}{n} Log C_e$ (4)

$q_e = \frac{RT}{b_T} ln K_T + \frac{RT}{b_T} ln C_e$ (5)

where K_L stands for the Langmuir constant (L/mg) and q_m is maximum adsorption capacity (mg/g). When $1/q_e$ was plotted against $1/C_e$, ln q_m against ln Ce were plotted (Fig. 4), the q_m and K_L values are obtained from the slope and intercept of the fitted line, respectively. K_F and n are the Freundlich constants. R (8.314 J mol^- K^-) is the universal gas constant, T in Kelvin is absolute temperature, b is the Temkin isotherm constant, and K_T (L/mg) is the Temkin binding constant.

2.3.3 Adsorption Kinetics

We have employed the pseudo-first-order and pseudo-second-order equations, shown in equations (6) and (7), respectively, to explained the kinetic properties of the adsorption process.

$log(q_e - q_t) = log q_e - (\frac{k_1}{2.303}) t$ (6)

$\frac{t}{q_t} = \frac{1}{k_2 q_e^2} + \frac{1}{q_e}$ (7)

where t is the contact time (min); k_1 is the first-order adsorption rate constant (min^{-1}), q_e and q_t is the adsorption capacity at equilibrium and time t (mg/g). When log (qe-qt) was plotted against t, the values of qe and k_1 were obtained from the slope and intercept of the fitted line, respectively. k_2 is the second-order adsorption rate constant (g/mg min). When t/qt was plotted against t, the values q_e and k_2 were computed using the slope and intercept of the plot, respectively.

2.3.4 Adsorption Thermodynamics

The analysis of thermodynamic parameters, such as standard Gibbs free energy (G), standard enthalpy (H), and standard entropy (S), determined the thermodynamic properties of the adsorption process. The relationships among ΔG, ΔH, and ΔS may be described as follows:

$\Delta G° = -RT ln K_L$ (8)

$$K_L = \frac{q_e}{C_e} \quad (9)$$

$$\Delta G^\circ = \Delta H^\circ - T\Delta S^\circ \quad (10)$$

$$lnK_L = \frac{\Delta S}{R} - \frac{\Delta H}{RT} \quad (11)$$

Where K_L is the distribution coefficient for the adsorption, qe is the adsorption capacity (mg/g), Ce is the dye concentration in solution at equilibrium (mmol/ml), T (K) is the temperature, and R (J mol^{-1} K^{-1}) the gas constant. The amounts of ΔH◦ and ΔS◦ could be identified by the slope and intercept of the solid line drawn using the plots of ln K_L versus 1/T.

3 Results and Discussion

3.1 Optimization of adsorption conditions

With the use of TiO_2 NPs, the drug and dye were adsorbed in a batch process with a specific amount of the adsorbate solution at room temperature. For the adsorption experiments, a 100-mL beaker was utilized, containing 50 mL of solutions with adsorbates at a concentration of 100 mg/L. We performed adsorption experiments across a spectrum of pH levels from 2 to 10, holding all other experimental parameters constant. Different concentrations of dye and drugs (ranging from 20 mg/L to 180 mg/L) were also examined. Various amounts of adsorbent were added to a solution containing a specific concentration of adsorbate. The objective was to examine the adsorption capacity and intensity under consistent temperature conditions. We assessed the adsorption mechanism by observing the adsorption of dye and drug molecules from a water-based solution onto the adsorbent over a range of time spans, from 0 to 200 minutes. Using a magnetic stirrer, we investigated the impact of different stirring rates, ranging from 200 to 1000 RPMs, as well as the influence of temperatures between 303 and 333 K.

3.1.1 Effect of Concentration

The study investigated the influence of different initial concentrations on the adsorption efficiency of MBD and GTF using TiO2 NPs. The results are illustrated in Fig. 4. The adsorption capacity demonstrated a positive correlation with the initial concentration. The equilibrium adsorption quantity (qe; mg/g) increased until the adsorbent reached saturation. At a specific concentration of adsorbate, the adsorption sites for each dose of adsorbent were nearly saturated, leaving only a few available. Understanding the concentration gradient of adsorbate can play a crucial role in driving the process of sorption [40].

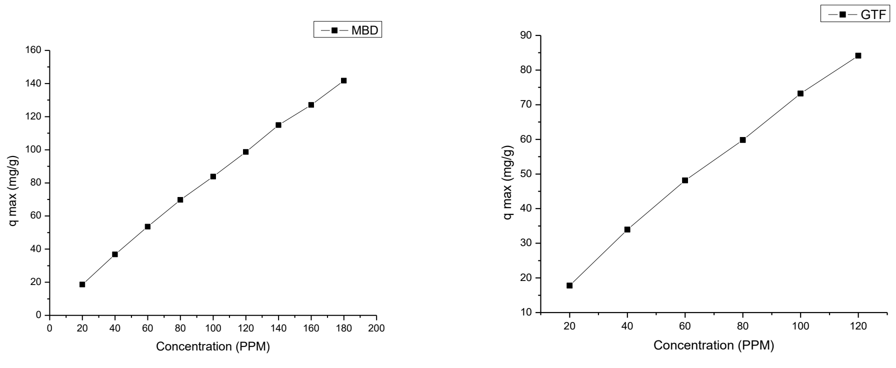

Fig. 4 Impact of initial MBD and GTF adsorbate concentrations

3.1.2 Effect of pH

The solution's pH and the adsorbent's surface charge play significant roles in the ionization and speciation of different contaminants. The pH of the solution has a significant effect on an adsorbent's adsorption capacity. We explored the impact of pH on adsorbate adsorption across pH levels of 2, 4, 6, 8, and 10, adjusting them using NaOH and HCl solutions. At pH 6, TiO2 removed MBD and GTF significantly more efficiently (Fig. 5). When a solution's pH rises from 6 to 12, dye and drug removal become much less effective. The reduced adsorption capacity observed at low pH levels could be attributed to the presence of hydrogen on the adsorbent surface, hindering the binding of ions to the active sites of the adsorbent. Electrostatic forces increase the concentration of positively charged dye ions on the negatively charged adsorbent surface at high pH levels [41].

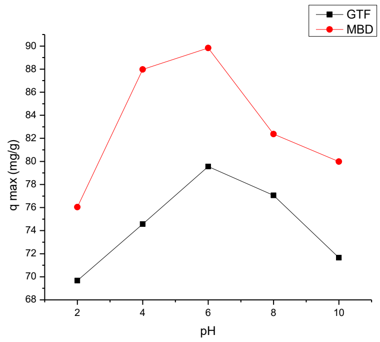

Fig. 5 Influence of pH on MBD & GTF sorption by TiO_2 NPs

3.1.3 Effect of dose

The number of adsorbent changes both the percentage of drug and dye removed (Fig. 6b) and the amount of dye and drug absorbed per unit weight of adsorbent (qe) (Fig. 6a). The size of the adsorbent particles influences adsorption because smaller particles have a larger surface area, resulting in increased adsorption [42]. We utilized various dosages of 0.02, 0.04, 0.06, 0.08, and 0.10 gm for MBD and GTF adsorption at ambient temperature and pH 6. As shown in Fig. 5b, when we increased the adsorbent dosage from 0.02 g/100 mL to 0.1 g/100 mL, the MBD and GTF adsorption efficiency increased from 77.63% and 68.89% to 93.17% and 79.86%, respectively.

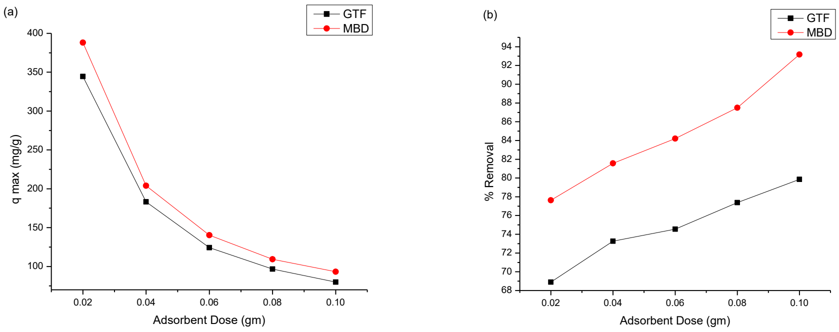

Fig. 6 Influence of adsorbent dose on MBD & GTF sorption by TiO_2 NPs

3.1.4 Effect of time

The adsorption quantity (qt) gradually increased over the first 45 and 100 minutes of stirring for MBD and GTF, respectively (Fig. 7). The adsorption performance remained unchanged.

Consequently, the adsorption process reached equilibrium after 45 and 100 minutes of stirring, respectively. The diffusion from the adsorbent's bulk to its surface regulates fast adsorption. The presence of enough surface area and open, active sites for dye and drug adsorption in the initial phases results in a high adsorption rate, but as reaction time grows, the active sites become saturated, resulting in a nearly constant adsorption efficiency. We determined the equilibrium time for TiO2 NPs to be 200 minutes [41].

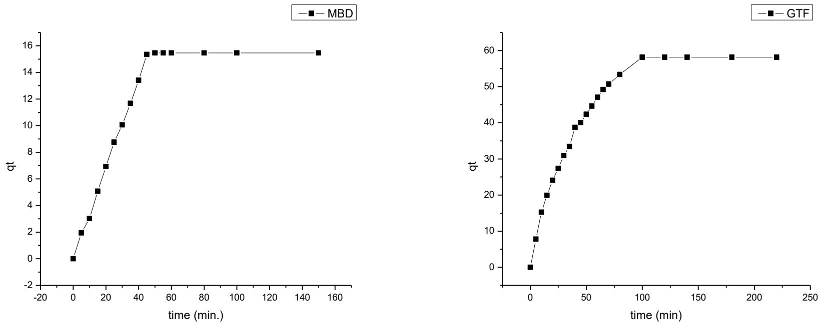

Fig. 7 Influence of contact time on MBD & GTF sorption by TiO_2 NPs

3.1.5 Effect of stirring rate

An investigation was conducted to examine the influence of different stirring rates, ranging from 200 to 1000 RPM, using 0.1 gm of adsorbent and maintaining a pH of 6. Enhanced dye and drug removal were achieved at 800 RPM (Fig. 8). By increasing the speeds, the adsorbate and adsorbent can come into closer contact, leading to an increase in adsorption [43].

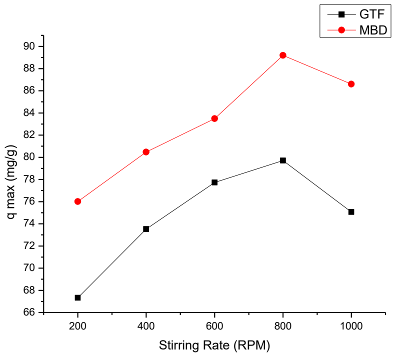

Fig. 8 Influence of stirring rate on MBD & GTF sorption by TiO_2 NPs

3.1.6 Effect of temperature

Use JLA to evaluate how temperature affects the adsorption of dye and drug. We conducted the experiments within a temperature range of 30 to 60 °C. Figure 9 shows how temperature affects TiO_2 NPs' MBD and GTF removal efficiencies. The sorption of the dye and drug decreased as the temperature increased. Reduced adsorptive pressure between adsorbate molecules and the active binding sites may be the cause of this [44]. As a consequence, among the temperatures examined, 30°C (room temperature) was shown to be the most effective for MBD and GTF sorption.

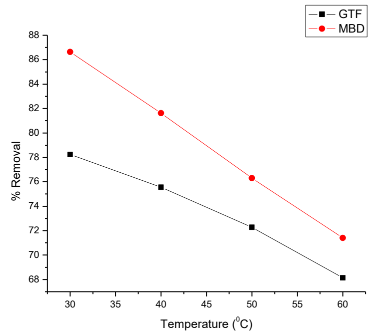

Fig. 9 Influence of temperatures on MBD & GTF sorption by TiO_2 NPs

3.2 Adsorption isotherms

Studying isotherms is important in adsorption modelling because it lets you see how the adsorbent materials (TiO_2 NPs) interact with the adsorbate substance. This approach contributes to a better understanding the adsorption process and makes calculating the adsorbent capacity easier. The study analyses experimental data on removing adsorbate from aqueous solutions at room temperature. We used the Langmuir, Freundlich, and Temkin isotherms to identify the best isotherm model for this specific application.

Table 2 The parameters for fitting the isothermal model for GTF and MBD adsorption onto TiO_2 NPs

Adsorption isotherm	**Parameters**	**Value**	
		MBD	**GTF**
Langmuir isotherm model	Q max (mg/g)	145.77	91.32
	K_L (L/mg)	0.1045	0.1076
	R_L	0.0872	0.0849
	R^2	0.9943	0.9904
Freundlich isotherm model	1/n	0.5841	0.5483
	K_f	17.072	11.982
	R^2	0.9901	0.9943
Temkin isotherm model	BT (J/mol)	36.11	23.244
	K_T(L/mg)	-0.1392	-0.2171
	R^2	0.9379	0.9547

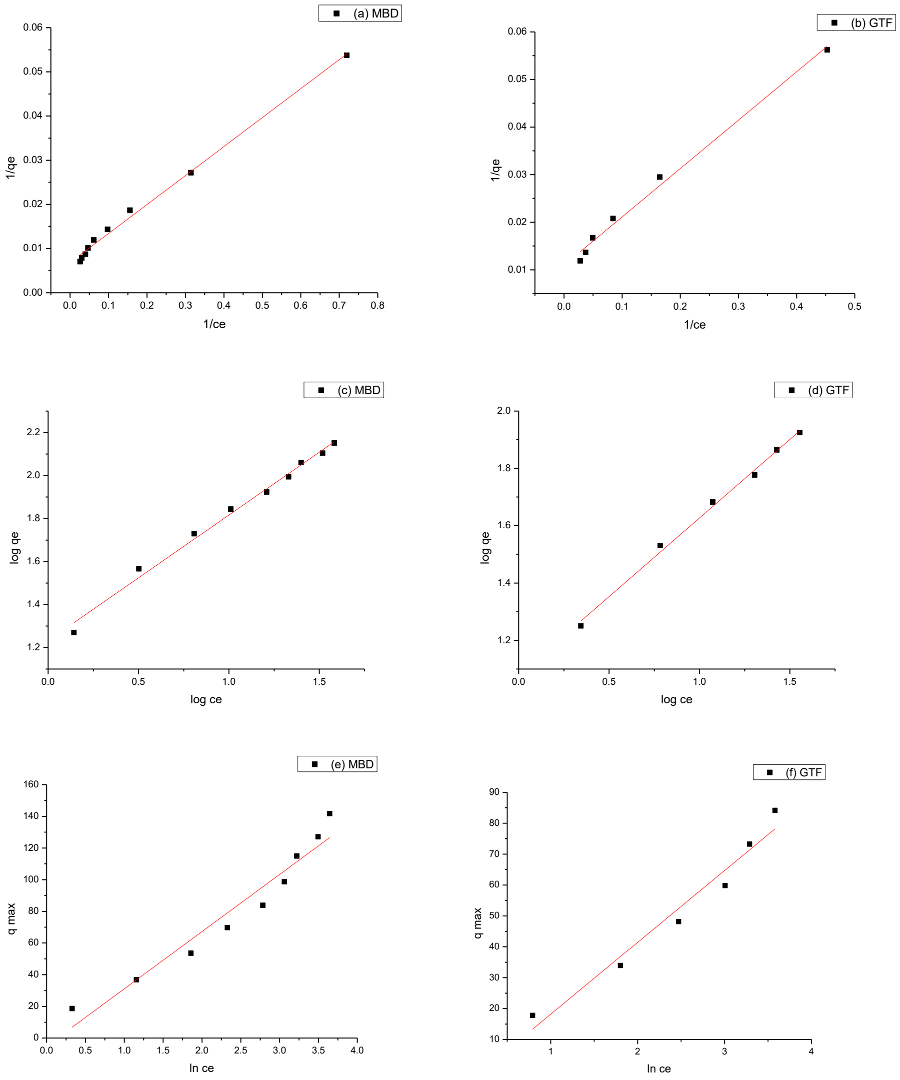

Fig. 10 Adsorption models for TiO_2 NPs include the (a), (b), Langmuir isotherm, (c), (d) Freundlich isotherm and (e), (f) Temkin isotherm

Table 2 and Fig. 10 display the results of the investigation, offering insights into the adsorption behaviour of MBD and GTF. The separation factor (R_L) is determined using the equation $R_L = 1/ (1 + K_L \times C_{In})$. It is an important element of the Langmuir isotherm and may predict the suitability of an adsorption system. When R_L is < 1, it indicates favourable adsorption. When R_L is > 1, it indicates unfavourable adsorption. When R_L equals 1, it indicates linear adsorption. Table 2 displays the computed RL. In the Langmuir isotherm, the maximum adsorption capacity for MBD was 145.77 mg/g, whereas for GTF, it was 91.32 mg/g. Notably, the Langmuir isotherm model exhibited a considerably higher R2 value compared to the Freundlich and Temkin isotherm models. This suggests that the Langmuir and Freundlich isotherm models provided a more precise depiction of the experimental data, implying that MBD and GTF adsorption onto TiO_2 NPs involved monolayer and multilayer adsorption processes, respectively. According to the Temkin isotherm model, the B_T values showed a positive trend, suggesting that the adsorption process may be exothermic.

3.3 Adsorption kinetics

We used pseudo-first-order and pseudo-second-order equations to analyze the kinetic data collected at ambient temperature to investigate the adsorption process.

Table 3 Parameters for fitting kinetic models to the adsorption of MBD and GTF on TiO_2 NPs

Kinetics	**Parameters**	**Value**	
		MBD	**GTF**
	qe, exp (mg/g)	83.81	73.21
Pseudo first order	qe, cal. (mg/g)	84.02	68.36
	k_1 (1/min)	-4.4×10^{-5}	-1.6×10^{-4}
	R^2	0.9973	0.9948
Pseudo second order	qe, cal. (mg/g)	19.96	68.54
	k_2 (g/mg min)	0.0017	0.0004
	R^2	0.8656	0.9745

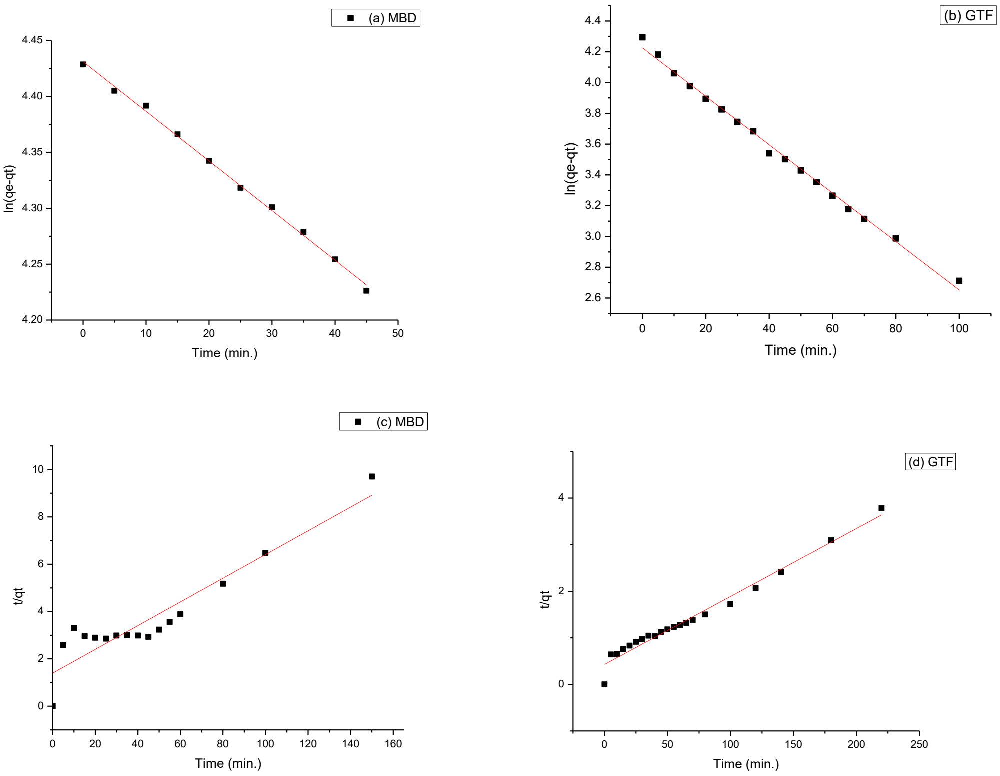

Fig. 11 Adsorption models for TiO_2 NPs includes kinetics Pseudo-first-order (a), (b) and Pseudo-second-order (c), (d)

Table 3 and Fig. 11 display the results of the kinetic investigations. Furthermore, the plots of ln(qe-qt) vs. t show a significant correlation between the experimental and calculated qe values. Specify the parameters for MBD and GTF. The pseudo-first-order kinetics model has correlation coefficients for the MBD and GTF that are above 0.99. The data analysis indicated that pseudo-first-order kinetics models are suitable for studying adsorption processes involving TiO_2 NPs.

3.4 Adsorption thermodynamic

The study of thermodynamic parameters, particularly ΔG◦, ΔH◦, and ΔS◦, helped determine the thermodynamic properties of MBD and GTF adsorption events. Table 4 reports the parameters, while Fig. 12 displays the relevant graphs.

Table 4 Thermodynamic parameters for the adsorption of MBD and GTF on TiO_2 NPs

Adsorbents	**Temperature (T)**	**ΔG◦ (KJ mol^{-1})**	**ΔH◦ (KJ mol^{-1})**	**ΔS◦ (J mol^{-1} K^{-1})**	**R^2**
MBD	303	-6.0054	-21.788	-52.253	0.9929
	313	-5.3749			
	323	-4.8636			
	333	-4.4428			
GTF	303	-3.6015	-10.636	-23.139	0.9927
	313	-3.4192			
	323	-3.1892			
	333	-2.9025			

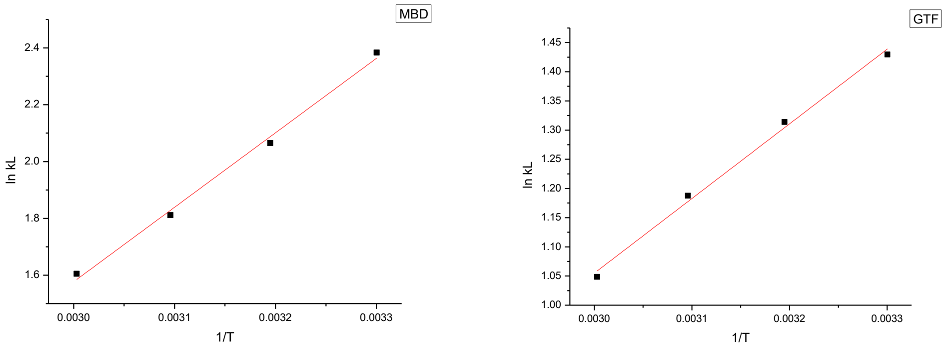

Fig. 12 The plot of ln K_L as a function of 1/T for the removal of MBD & GTF by TiO_2 NPs

Adsorption of MBD and GTF onto TiO_2 NPs was shown to be spontaneous and effective, as evidenced by negative ΔG◦ values at temperatures ranging from 303–333 K. These values increased with temperature, demonstrating that adsorption is more effective at lower temperatures and less clear at higher ones. The negative value of ΔH◦ indicates an exothermic adsorption process. Negative ΔS◦ values indicate reduced disorder at the solid/solution interface during adsorption, leading to a decrease in adsorption capacity when dye and drug molecules are removed from the adsorbent.

3.5 Characterization of TiO_2 NPs

3.5.1 X-Ray Diffraction analysis

Fig. 13 presents XRD data of TiO_2 NPs produced with MO extract across a 2θ range of 10°–70°. The XRD pattern of the TiO_2 NPs sample shows a main orientation peak at 2θ = 25.30°, with additional strong peaks at 37.90°, 47.97°, 54.52°, and 62.45°. The planes of (101), (004), (200), (105), and (204) are appropriate with JCPDS card no. 21-1272. Each of these peaks corresponded to the tetragonal crystal structure of TiO_2 NPs. We use the Scherrer equation, expressed by the following formula, to calculate the average crystallite size:

$$D = \frac{K\lambda}{\beta Cos\theta} \quad (12)$$

In the given context, the variables are as follows: X-ray wavelength (λ) = 0.1541 nm, FWHM (full width at half maximum) (β), diffraction angle (θ), d-spacing (d), and particle diameter size (D). We determined the mean size of TiO_2 NPs to be 105.27 nm.

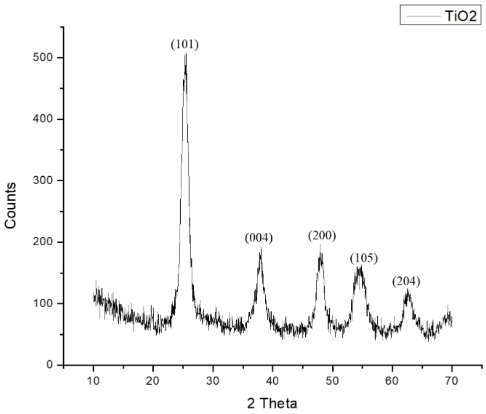

Fig. 13 XRD pattern of TiO_2 NPs

3.5.2 FESEM and EDX analysis

We investigated the structure of the TiO_2 NPs using FESEM, as shown in Fig. 14 a, c, and e. After examining the FESEM images, it was revealed that the TiO_2 NPs generated using the green method had varying magnification. The photos revealed a spherical and irregular nanostructure with a highly porous network. Additionally, the aggregation of NPs was minimized by the MO extract, which served as both a capping and reducing agent. There was a slight observation of powder particles being agglomerated.

We used EDX analysis to determine the composition of the produced TiO_2 NPs. Figure 14b confirms the presence of titanium and oxygen. When dye and drug molecules load onto the surface of TiO_2 NPs after MBD and GTF adsorption, the surface becomes more compact and less porous (Fig. 14 d, f). On the surface of TiO_2 NPs, the EDX analysis identified sulfur (S) and carbon (C) from the molecular structure of MBD [45], as well as nitrogen (N), fluorine (F), and carbon (C) from the molecular structure of GTF. This is illustrated in Figs. 14d and f.

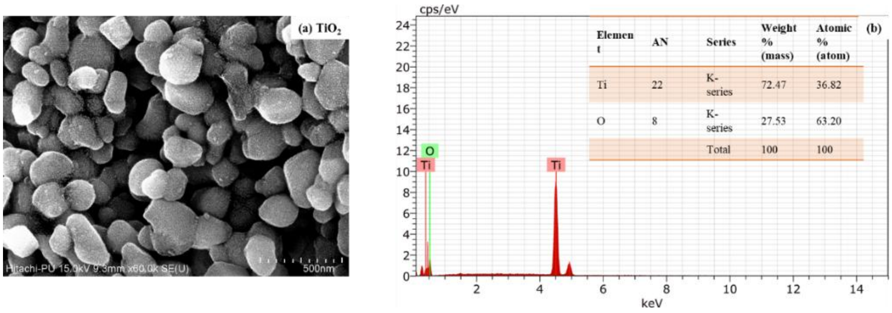

Element	AN	Series	Weight % (mass)	Atomic % (atom)
Ti	22	K-series	72.47	36.82
O	8	K-series	27.53	63.20
		Total	100	100

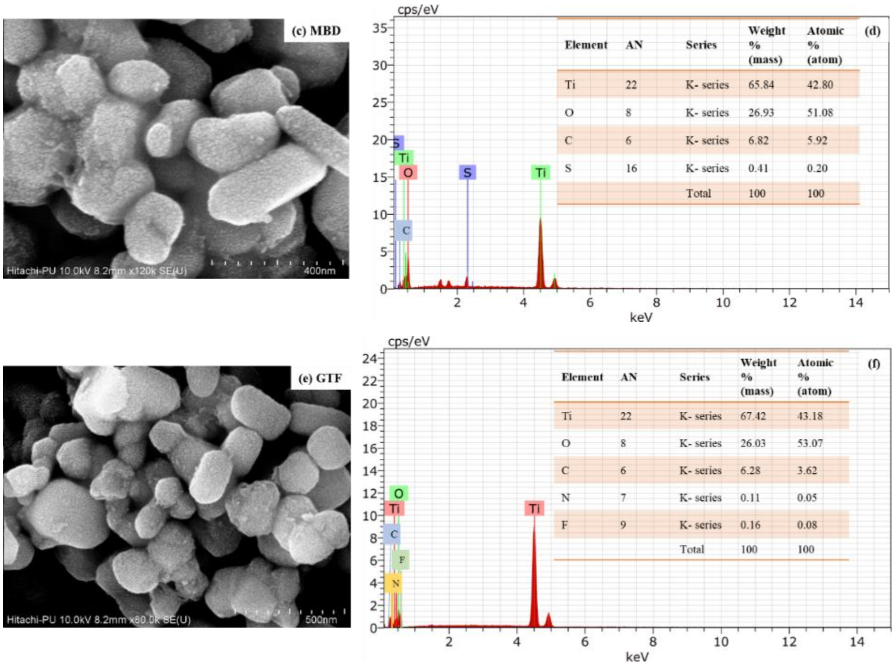

(d)

Element	AN	Series	Weight % (mass)	Atomic % (atom)
Ti	22	K- series	65.84	42.80
O	8	K- series	26.93	51.08
C	6	K- series	6.82	5.92
S	16	K- series	0.41	0.20
		Total	100	100

(f)

Element	AN	Series	Weight % (mass)	Atomic % (atom)
Ti	22	K- series	67.42	43.18
O	8	K- series	26.03	53.07
C	6	K- series	6.28	3.62
N	7	K- series	0.11	0.05
F	9	K- series	0.16	0.08
		Total	100	100

Fig. 14 FESEM - EDX image of (a, b) before and (c, d, e, f) after adsorption

3.5.3 TEM analysis

It was confirmed by TEM analysis (Fig. 15a) that the TiO_2 NPs made using the green route had the right particle size and shape, with a uniform distribution and a spherical shape. The TEM image estimates the particle size to be approximately 100 nm. The SAED picture (Fig. 15b) shows that the diffraction rings align with the XRD pattern. This confirms that the TiO_2 NPs are crystallized and in the anatase phase. Based on HR-TEM observations in Fig. 15 c, the TiO_2 NPs possess a lattice structure [46].

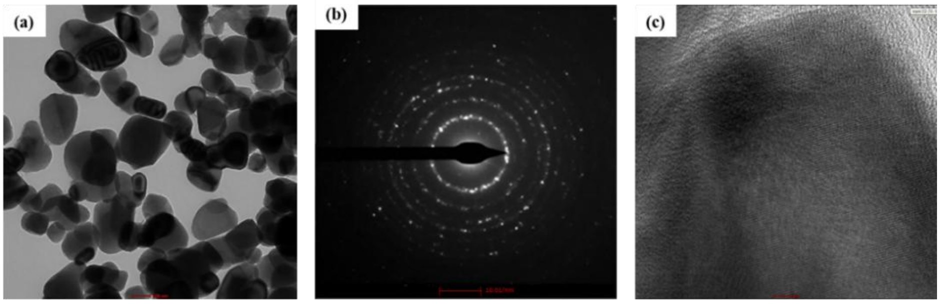

Fig. 15 TEM-SAED image of TiO_2 NPs

3.5.4 FTIR analysis

FTIR analysis was used to identify many different functional groups of the TiO_2 NPs before and after adsorption (Shown in Fig. 16). The frequency at which the CH_3 stretched peaked was 2925.33 cm^{-1}. The TiO_2 NPs displayed a broad absorption band at 3399.32 $cm^{-1,}$ representing the hydroxyl (O-H) group [26]. The bending vibrations of O-H produced by adsorbed water molecules were identified as the narrow band at 1630.38 cm^{-1} [47]. Titanium carboxylate, made from TTIP, peaked at 1630.38 cm^{-1}, whereas C-O stretching alcohols, carboxylic acids, esters, and ethers peaked at 1145.80 cm^{-1} [48]. The specific signal for TiO_2 NPs seen in the FTIR spectra below 1000 cm^{-1} was attributed to Ti-O-Ti vibration [46], while the band at 493 cm^{-1} has been identified as the Ti-O-Ti bridging and Ti-O stretching modes [49].

The IR spectra of MBD and GTF are complex because of several functional groups. For MBD adsorption, the peak at 3401.34 cm^{-1} (indicating the stretching vibration of -CH- aromatic and –CH_3 groups of MBD) has appeared with the MBD bands for the C=N central ring stretching at 1618.89 cm^{-1}, the C=C side ring stretching at 1492.04 cm^{-1} and the Ar-N stretching at 1339.62 cm^{-1} [50]. For GTF adsorption, the peak at 3600.64 cm^{-1} for OH and NH stretch, at 3393.14 cm^{-1} for OH-bonded, and the different peaks at 1632.10 cm^{-1} and 1468.47 cm^{-1} for pyridine C=O stretch, quinoline ring C-C and C-N stretch, peak at 1282.07 cm^{-1} and 1093.42 cm^{-1} for C-F and C-O stretching and bending, respectively.

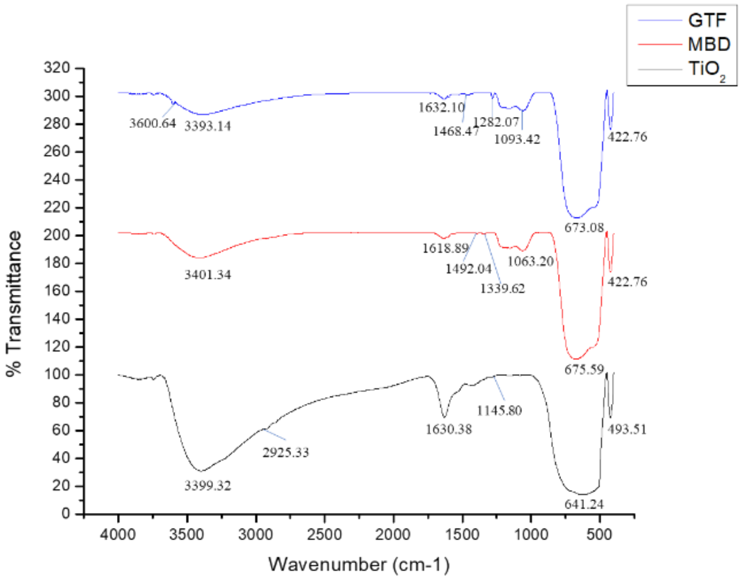

Fig. 16 FTIR spectra of TiO_2 NPs before and after adsorption

3.5.5 Particle size and BET analysis

Most particles range in size from 100 to 140 nm, with an average length of around 129.38 nm. Fig. 17 shows the size distribution of the NPs in the SEM image, ranging from 60 to 260 nm, plotted using ImageJ software. The majority of the NPs fall within the 100–140 nm range. The TiO_2 NPs showed greater stability in the recent study on green synthesis, with a particle size of 110.84 nm that aligned closely with the TEM results.

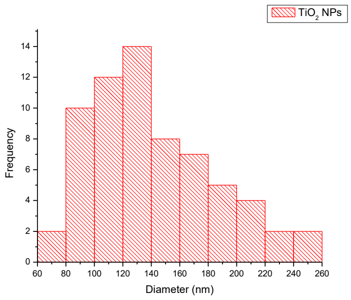

Fig. 17 Particle size distribution of TiO_2 NPs

We assessed the surface area of the synthesized TiO_2 NPs using a BET surface area analyzer. Additional parameters, like pore size and pore volume, were determined through BJH analysis. Table 5 provides a comparison of the surface area characteristics of TiO_2 NPs prepared using various plant extracts.

Table 5 Comparison of BET analysis with others

Adsorbents	**Surface area (m^2/g)**	**Pore volume (cc/g)**	**Pore size (nm)**	**References**
TiO_2 NPs (Acorus calamus Leaf)	7.04	5.701	4.92	[30]
TiO_2 NPs (Micrococcus lylae)	21.3 ± 0.7	-	1.5	[51]
TiO_2 NPs (Aloe vera leaves)	19.12	-	-	[52]
TiO_2 NPs (Moringa oleifera leaf)	34.127	0.231	4.998	Present study

3.6 Regeneration cycles

The TiO_2 NPs do not dissolve in water or alcohol. Adding a pollutant-rich adsorbent to distilled water allowed for the recovery of adsorbates through simple distillation. We meticulously cleansed the residual solid with acetone and distilled water. We then heated it at 400°C in muffle furnaces to prepare it for reuse. As shown in Fig. 18, the catalyst demonstrated consistent reusability and effectiveness over five cycles of recovery and reuse.

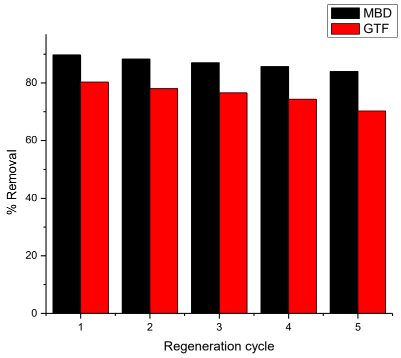

Fig. 18 MBD & GTF removal by regenerated TiO_2 NPs

4 Conclusion

Green nanotechnology has gained significant importance recently for its role in reducing harmful reagents and its cost-effective production of valuable products. Creating TiO_2 NPs through green synthesis offers a more environmentally friendly, cost-effective, and efficient alternative to conventional approaches like the sol-gel technique. This investigation synthesized TiO_2 NPs using leaf extract (MO). The distinct peaks observed in the XRD and TEM images revealed the high purity and crystallinity of the anatase form of TiO_2 NPs. Furthermore, we conducted confirmation of the TiO_2 NPs via FTIR, EDX, BET, and FESEM analyses. The nanoparticles produced had an average particle size of around 100 nm, determined through three different methods: Scherrer's formula from XRD (105.27 nm), TEM (110.84 nm), and FESEM (129.38 nm), with the figures in supports representing the particle sizes. These nanoparticles were made green using natural, renewable, and eco-friendly materials. The study shows they have a good capacity for

MBD of 145.77 mg/g and a GTF of 91.32 mg/g for adsorption. This system is suitable for water purification and industrial effluent treatment.

References

1. Hemmati, F., Norouzbeigi, R., Sarbisheh, F., Shayesteh, H.: Malachite green removal using modified sphagnum peat moss as a low-cost biosorbent: Kinetic, equilibrium and thermodynamic studies. Journal of the Taiwan Institute of Chemical Engineers. 58, 482–489 (2016). https://doi.org/10.1016/j.jtice.2015.07.004
2. Yagub, M.T., Sen, T.K., Afroze, S., Ang, H.M.: Dye and its removal from aqueous solution by adsorption: A review. Advances in Colloid and Interface Science. 209, 172–184 (2014). https://doi.org/10.1016/j.cis.2014.04.002
3. Nadal, M., Marquès, M., Mari, M., Domingo, J.L.: Climate change and environmental concentrations of POPs: A review. Environmental Research. 143, 177–185 (2015). https://doi.org/10.1016/j.envres.2015.10.012
4. Zhao, B., Sun, X., Wang, L., Zhao, L., Zhang, Z., Li, J.: Adsorption of methyl orange from aqueous solution by composite magnetic microspheres of chitosan and quaternary ammonium chitosan derivative. Chinese Journal of Chemical Engineering. 27, 1973–1980 (2019). https://doi.org/10.1016/j.cjche.2018.12.014
5. Jegatheesan, V., Pramanik, B.K., Chen, J., Navaratna, D., Chang, C.-Y., Shu, L.: Treatment of textile wastewater with membrane bioreactor: A critical review. Bioresource Technology. 204, 202–212 (2016). https://doi.org/10.1016/j.biortech.2016.01.006
6. Popaliya, M., Mishra, A.: Modified zeolite as an adsorbent for dyes, drugs, and heavy metal removal: a review. Int. J. Environ. Sci. Technol. (2022). https://doi.org/10.1007/s13762-022-04603-z
7. Tharaneedhar, V., Senthil Kumar, P., Saravanan, A., Ravikumar, C., Jaikumar, V.: Prediction and interpretation of adsorption parameters for the sequestration of methylene blue dye from aqueous solution using microwave assisted corncob activated carbon. Sustainable Materials and Technologies. 11, 1–11 (2017). https://doi.org/10.1016/j.susmat.2016.11.001
8. Saratale, R.G., Rajesh Banu, J., Shin, H.-S., Bharagava, R.N., Saratale, G.D.: Textile Industry Wastewaters as Major Sources of Environmental Contamination: Bioremediation Approaches for Its Degradation and Detoxification. In: Saxena, G. and Bharagava, R.N. (eds.) Bioremediation of Industrial Waste for Environmental Safety. pp. 135–167. Springer Singapore, Singapore (2020)
9. Kataria, N., Garg, V.K.: Application of EDTA modified Fe3O4/sawdust carbon nanocomposites to ameliorate methylene blue and brilliant green dye laden water. Environmental Research. 172, 43–54 (2019). https://doi.org/10.1016/j.envres.2019.02.002
10. Chen, F., Yang, Q., Yao, F., Wang, S., Sun, J., An, H., Yi, K., Wang, Y., Zhou, Y., Wang, L., Li, X., Wang, D., Zeng, G.: Visible-light photocatalytic degradation of multiple antibiotics by AgI nanoparticle-sensitized Bi5O7I microspheres: Enhanced interfacial charge transfer based on Z-scheme heterojunctions. Journal of Catalysis. 352, 160–170 (2017). https://doi.org/10.1016/j.jcat.2017.04.032
11. Gothwal, R., Shashidhar, T.: Antibiotic Pollution in the Environment: A Review. CLEAN Soil Air Water. 43, 479–489 (2015). https://doi.org/10.1002/clen.201300989
12. Arhoutane, M.R., Kaichouh, G., Yahya, M.S., El Karbane, M., Chakchak, H., El Kacemi, K.: Elimination of gatifloxacin from water: Treatment by electro-Fenton process and highlighting of a biological post-treatment. Mediterr.J.Chem.,. 8, 308–319 (2019). https://doi.org/10.13171/mjc841906066mra
13. Bengtsson-Palme, J., Kristiansson, E., Larsson, D.G.J.: Environmental factors influencing the development and spread of antibiotic resistance. FEMS Microbiology Reviews. 42, (2018). https://doi.org/10.1093/femsre/fux053

14. Xu, R., Zheng, R., Wang, Y., Ma, R., Tong, G., Wei, X., Feng, D., Hu, K.: Transcriptome analysis to elucidate the toxicity mechanisms of fenvalerate, sulfide gatifloxacin, and ridomil on the hepatopancreas of Procambarus clarkii. Fish & Shellfish Immunology. 116, 140–149 (2021). https://doi.org/10.1016/j.fsi.2021.07.004
15. Chavali, M.S., Nikolova, M.P.: Metal oxide nanoparticles and their applications in nanotechnology. SN Appl. Sci. 1, 607 (2019). https://doi.org/10.1007/s42452-019-0592-3
16. Dubey, R.S.: Temperature-dependent phase transformation of TiO2 nanoparticles synthesized by sol-gel method. Materials Letters. 215, 312–317 (2018). https://doi.org/10.1016/j.matlet.2017.12.120
17. Hingrajiya, R.D., Patel, M.P.: Fe3O4 modified chitosan based co-polymeric magnetic composite hydrogel: Synthesis, characterization and evaluation for the removal of methylene blue from aqueous solutions. International Journal of Biological Macromolecules. 244, 125251 (2023). https://doi.org/10.1016/j.ijbiomac.2023.125251
18. Wang, D., Xie, K., Wang, Y., Cheng, S.: A Non-aqueous Hybrid Supercapacitor with Porous Anatase TiO Nanoparticles Anode and Activated Carbon Cathode. International Journal of Electrochemical Science. 11, 9776–9782 (2016). https://doi.org/10.20964/2016.12.15
19. Selvakumar, M., Bhat, D.K.: Microwave synthesized nanostructured TiO2-activated carbon composite electrodes for supercapacitor. Applied Surface Science. 263, 236–241 (2012). https://doi.org/10.1016/j.apsusc.2012.09.036
20. Guimarães, J.L., Abbate, M., Betim, S.B., Alves, M.C.M.: Preparation and characterization of TiO2 and V2O5 nanoparticles produced by ball-milling. Journal of Alloys and Compounds. 352, 16–20 (2003). https://doi.org/10.1016/S0925-8388(02)01112-X
21. Zikriya, M., Nadaf, Y.F., Bharathy, P.V., Renuka, C.G.: Luminescent characterization of rare earth Dy3+ ion doped TiO2 prepared by simple chemical co-precipitation method. Journal of Rare Earths. 37, 24–31 (2019). https://doi.org/10.1016/j.jre.2018.05.012
22. Lee, D.-H., Swain, B., Shin, D., Ahn, N.-K., Park, J.-R., Park, K.-S.: One-pot wet chemical synthesis of fluorine-containing TiO2 nanoparticles with enhanced photocatalytic activity. Materials Research Bulletin. 109, 227–232 (2019). https://doi.org/10.1016/j.materresbull.2018.09.027
23. Khade, G.V., Suwarnkar, M.B., Gavade, N.L., Garadkar, K.M.: Green synthesis of TiO2 and its photocatalytic activity. J Mater Sci: Mater Electron. 26, 3309–3315 (2015). https://doi.org/10.1007/s10854-015-2832-7
24. Nabi, G., Ain, Q.-U.-, Tahir, M.B., Nadeem Riaz, K., Iqbal, T., Rafique, M., Hussain, S., Raza, W., Aslam, I., Rizwan, M.: Green synthesis of TiO $_2$ nanoparticles using lemon peel extract: their optical and photocatalytic properties. International Journal of Environmental Analytical Chemistry. 102, 434–442 (2022). https://doi.org/10.1080/03067319.2020.1722816
25. Ahmad, W., Jaiswal, K.K., Soni, S.: Green synthesis of titanium dioxide (TiO $_2$) nanoparticles by using *Mentha arvensis* leaves extract and its antimicrobial properties. Inorganic and Nano-Metal Chemistry. 50, 1032–1038 (2020). https://doi.org/10.1080/24701556.2020.1732419
26. Al-Shabib, N.A., Husain, F.M., Qais, F.A., Ahmad, N., Khan, A., Alyousef, A.A., Arshad, M., Noor, S., Khan, J.M., Alam, P., Albalawi, T.H., Shahzad, S.A.: Phyto-Mediated Synthesis of Porous Titanium Dioxide Nanoparticles From Withania somnifera Root Extract: Broad-Spectrum Attenuation of Biofilm and Cytotoxic Properties Against HepG2 Cell Lines. Front. Microbiol. 11, 1680 (2020). https://doi.org/10.3389/fmicb.2020.01680
27. Santhoshkumar, T., Rahuman, A.A., Jayaseelan, C., Rajakumar, G., Marimuthu, S., Kirthi, A.V., Velayutham, K., Thomas, J., Venkatesan, J., Kim, S.-K.: Green synthesis of titanium dioxide nanoparticles using Psidium guajava extract and its antibacterial and antioxidant properties. Asian Pacific Journal of Tropical Medicine. 7, 968–976 (2014). https://doi.org/10.1016/S1995-7645(14)60171-1
28. Kim, J.S., Kuk, E., Yu, K.N., Kim, J.-H., Park, S.J., Lee, H.J., Kim, S.H., Park, Y.K., Park, Y.H., Hwang, C.-Y., Kim, Y.-K., Lee, Y.-S., Jeong, D.H., Cho, M.-H.: Antimicrobial effects of silver nanoparticles.

Nanomedicine: Nanotechnology, Biology and Medicine. 3, 95–101 (2007). https://doi.org/10.1016/j.nano.2006.12.001

29. Aswathy Aromal, S., Philip, D.: Green synthesis of gold nanoparticles using Trigonella foenum-graecum and its size-dependent catalytic activity. Spectrochimica Acta Part A: Molecular and Biomolecular Spectroscopy. 97, 1–5 (2012). https://doi.org/10.1016/j.saa.2012.05.083
30. Ansari, A., Siddiqui, V.U., Rehman, W.U., Akram, Md.K., Siddiqi, W.A., Alosaimi, A.M., Hussein, M.A., Rafatullah, M.: Green Synthesis of TiO2 Nanoparticles Using Acorus calamus Leaf Extract and Evaluating Its Photocatalytic and In Vitro Antimicrobial Activity. Catalysts. 12, 181 (2022). https://doi.org/10.3390/catal12020181
31. Rajendhiran, R., Deivasigamani, V., Palanisamy, J., Masan, S., Pitchaiya, S.: Terminalia catappa and carissa carandas assisted synthesis of Tio2 nanoparticles – A green synthesis approach. Materials Today: Proceedings. 45, 2232–2238 (2021). https://doi.org/10.1016/j.matpr.2020.10.223
32. Thamima, M., Karuppuchamy, S.: Biosynthesis of Titanium Dioxide and Zinc Oxide Nanoparticles from Natural Sources: A Review. Adv Sci Engng Med. 7, 18–25 (2015). https://doi.org/10.1166/asem.2015.1648
33. Rajakumar, G., Rahuman, A.A., Jayaseelan, C., Santhoshkumar, T., Marimuthu, S., Kamaraj, C., Bagavan, A., Zahir, A.A., Kirthi, A.V., Elango, G., Arora, P., Karthikeyan, R., Manikandan, S., Jose, S.: Solanum trilobatum extract-mediated synthesis of titanium dioxide nanoparticles to control Pediculus humanus capitis, Hyalomma anatolicum anatolicum and Anopheles subpictus. Parasitol Res. 113, 469–479 (2014). https://doi.org/10.1007/s00436-013-3676-9
34. Roopan, S.M., Bharathi, A., Prabhakarn, A., Abdul Rahuman, A., Velayutham, K., Rajakumar, G., Padmaja, R.D., Lekshmi, M., Madhumitha, G.: Efficient phyto-synthesis and structural characterization of rutile TiO2 nanoparticles using Annona squamosa peel extract. Spectrochimica Acta Part A: Molecular and Biomolecular Spectroscopy. 98, 86–90 (2012). https://doi.org/10.1016/j.saa.2012.08.055
35. Velayutham, K., Rahuman, A.A., Rajakumar, G., Santhoshkumar, T., Marimuthu, S., Jayaseelan, C., Bagavan, A., Kirthi, A.V., Kamaraj, C., Zahir, A.A., Elango, G.: Evaluation of Catharanthus roseus leaf extract-mediated biosynthesis of titanium dioxide nanoparticles against Hippobosca maculata and Bovicola ovis. Parasitol Res. 111, 2329–2337 (2012). https://doi.org/10.1007/s00436-011-2676-x
36. Nwanya, A.C., Ugwuoke, P.E., Ejikeme, P.M., Oparaku, O.U., Ezema, F.I.: Jathropha Curcas and Citrus Aurantium Leaves Dye Extract for Use in Dye Sensitized Solar Cell with TiO Films. International Journal of Electrochemical Science. 7, 11219–11235 (2012). https://doi.org/10.1016/S1452-3981(23)16938-0
37. Rajakumar, G., Rahuman, A.A., Priyamvada, B., Khanna, V.G., Kumar, D.K., Sujin, P.J.: Eclipta prostrata leaf aqueous extract mediated synthesis of titanium dioxide nanoparticles. Materials Letters. 68, 115–117 (2012). https://doi.org/10.1016/j.matlet.2011.10.038
38. Marimuthu, S., Rahuman, A.A., Jayaseelan, C., Kirthi, A.V., Santhoshkumar, T., Velayutham, K., Bagavan, A., Kamaraj, C., Elango, G., Iyappan, M., Siva, C., Karthik, L., Rao, K.V.B.: Acaricidal activity of synthesized titanium dioxide nanoparticles using Calotropis gigantea against Rhipicephalus microplus and Haemaphysalis bispinosa. Asian Pacific Journal of Tropical Medicine. 6, 682–688 (2013). https://doi.org/10.1016/S1995-7645(13)60118-2
39. Yaseen Sharaf Zeebaree, A., Yaseen Sharaf Zeebaree, S., Rashid, R.F., Ismail Haji Zebari, O., Albarwry, A.J.S., Ali, A.F., Yaseen Sharaf Zebari, A.: Sustainable engineering of plant-synthesized TiO2 nanocatalysts: Diagnosis, properties and their photocatalytic performance in removing of methylene blue dye from effluent. A review. Current Research in Green and Sustainable Chemistry. 5, 100312 (2022). https://doi.org/10.1016/j.crgsc.2022.100312
40. Alghamdi, W.M., El Mannoubi, I.: Investigation of Seeds and Peels of Citrullus colocynthis as Efficient Natural Adsorbent for Methylene Blue Dye. Processes. 9, 1279 (2021). https://doi.org/10.3390/pr9081279

41. Deniz, F., Kepekci, R.A.: Bioremoval of Malachite green from water sample by forestry waste mixture as potential biosorbent. Microchemical Journal. 132, 172–178 (2017). https://doi.org/10.1016/j.microc.2017.01.015
42. Sri Devi, V., Sudhakar, B., Prasad, K., Jeremiah Sunadh, P., Krishna, M.: Adsorption of Congo red from aqueous solution onto Antigonon leptopus leaf powder: Equilibrium and kinetic modeling. Materials Today: Proceedings. 26, 3197–3206 (2020). https://doi.org/10.1016/j.matpr.2020.02.715
43. Saha, P., Chowdhury, S., Gupta, S., Kumar, I.: Insight into adsorption equilibrium, kinetics and thermodynamics of Malachite Green onto clayey soil of Indian origin. Chemical Engineering Journal. 165, 874–882 (2010). https://doi.org/10.1016/j.cej.2010.10.048
44. Saravanan, P., Josephraj, J., Thillainayagam, B.P., Ravindiran, G.: Evaluation of the adsorptive removal of cationic dyes by greening biochar derived from agricultural bio-waste of rice husk. Biomass Conv. Bioref. 13, 4047–4060 (2023). https://doi.org/10.1007/s13399-021-01415-y
45. Popaliya, M.R., Mishra, M., Mishra, A.: Removal of cationic dyes onto java plum leaves ash: adsorption isotherms, kinetics, thermodynamic and characterizations. Chem. Pap. 77, 7881–7901 (2023). https://doi.org/10.1007/s11696-023-03037-2
46. Saranya, K.S., Vellora Thekkae Padil, V., Senan, C., Pilankatta, R., Saranya, K., George, B., Wacławek, S., Černík, M.: Green Synthesis of High Temperature Stable Anatase Titanium Dioxide Nanoparticles Using Gum Kondagogu: Characterization and Solar Driven Photocatalytic Degradation of Organic Dye. Nanomaterials. 8, 1002 (2018). https://doi.org/10.3390/nano8121002
47. Yao, P., Zhong, S., Shen, Z.: TiO_2 /Halloysite Composites Codoped with Carbon and Nitrogen from Melamine and Their Enhanced Solar-Light-Driven Photocatalytic Performance. International Journal of Photoenergy. 2015, 1–8 (2015). https://doi.org/10.1155/2015/605690
48. Pushpamalini, T., Keerthana, M., Sangavi, R., Nagaraj, A., Kamaraj, P.: Comparative analysis of green synthesis of TiO2 nanoparticles using four different leaf extract. Materials Today: Proceedings. 40, S180–S184 (2021). https://doi.org/10.1016/j.matpr.2020.08.438
49. Sethy, N.K., Arif, Z., Mishra, P.K., Kumar, P.: Green synthesis of TiO2 nanoparticles from Syzygium cumini extract for photo-catalytic removal of lead (Pb) in explosive industrial wastewater. Green Processing and Synthesis. 9, 171–181 (2020). https://doi.org/10.1515/gps-2020-0018
50. Manea, Y.K., Khan, A.M.: Enhanced photocatalytic degradation of methylene blue and adsorption of metal ions by SDS-TiP nanocomposite. SN Appl. Sci. 1, 821 (2019). https://doi.org/10.1007/s42452-019-0817-5
51. Fulekar, J., Dutta, D.P., Pathak, B., Fulekar, M.H.: Novel microbial and root mediated green synthesis of TiO_2 nanoparticles and its application in wastewater remediation. J of Chemical Tech & Biotech. 93, 736–743 (2018). https://doi.org/10.1002/jctb.5423
52. Sonker, R.K., Hitkari, G., Sabhajeet, S.R., Sikarwar, S., Rahul, Singh, S.: Green synthesis of TiO2 nanosheet by chemical method for the removal of Rhodamin B from industrial waste. Materials Science and Engineering: B. 258, 114577 (2020). https://doi.org/10.1016/j.mseb.2020.114577

Declaration of Competing Interest

- Consent to participate Not applicable.
- Consent to publish is Not applicable
- The author(s) declared no potential conflicts of interest with respect to the research, authorship, and/or publication of this article, and the authors also declare that they have no known competing financial interests or personal relationships that could have appeared to influence the work reported in this paper.

Acknowledgments

The authors gratefully acknowledge sample analysis support received from the Sophisticated Instrumentation Centre for Applied Research and Testing (SICART), Vallabh Vidyanagar, Gujarat and Sophisticated Analytical Instrumentation Facility (SAIF & CIL), Chandigarh, Punjab. One of the authors (MRP) is grateful to SHODH ScHeme of Developing High Quality Research (KCG/SHODH/2020-21), Knowledge Consortium of Gujarat, Government of Gujarat for the scholarship.

Scholarship

SHODH - ScHeme of Developing High-Quality Research, Knowledge Consortium of Gujarat, (Education Department, Government of Gujarat. Letter Reference no: KCG/SHODH/2020-21/ & Grant number: 202010820024.

Author Contributions

Dr. Kinnari Bhatt and Dr. Arvnabh Mishra has given guidance & idea about this work, and he has supervised, monitored, and revised the manuscript. Meera R. Popaliya and Keval R. Rana has collected data, designed the manuscript and written the main text, and revised the manuscript. All authors have read and agreed to the published version of the manuscript.

Ethical Approval

We hereby declare that this work is original and not copied from anywhere else. We approve that this work is not submitted in this language or any other language to any other journal nor it is submitted for simultaneous consideration.

Data Availability

The datasets generated during and/or analysed during the current study are not publicly available due to privacy concerns but may be available from the corresponding author upon reasonable request.